Contents lists available at ScienceDirect

Solar Energy Materials and Solar Cells

journal homepage: www.elsevier.com/locate/solmat

A study of the hydration and dehydration transitions of $SrCl_2$ hydrates for use in heat storage

Melian A.R. Blijlevens [a], Natalia Mazur [b], Wessel Kooijman [a], Hartmut R. Fischer [c], Henk P. Huinink [b,**], Hugo Meekes [a], Elias Vlieg [a,*]

[a] *Radboud University, Institute for Molecules and Materials, Heyendaalseweg 135, 6525, ED, Nijmegen, the Netherlands*
[b] *Technical University Eindhoven, P.O. Box 513, Department of Applied Physics, 5600, MB, Eindhoven, the Netherlands*
[c] *Netherlands Organization for Applied Scientific Research (TNO), High Tech Campus 25, 5656, AE, Eindhoven, the Netherlands*

ARTICLE INFO

ABSTRACT

We have experimentally determined the main thermodynamic properties of $SrCl_2$, a potentially promising salt for thermochemical heat storage. We found a high energy density of 2.4 ± 0.1 GJ/m^3 and proved full cyclability for at least 10 cycles going from the anhydrate to the hexahydrate without chemical degradation. We have experimentally determined the thermodynamic equilibria for each individual transition and the corresponding metastable zones. We find that the metastable zone is widest for the anhydrate to monohydrate transition and decreases with each subsequent hydration step. We have also established that the observed nucleation kinetics are highly dependent on the preparation of the sample. Depending on the preparation conditions, some seeds of the precursor phase can remain in the sample thereby influencing the induction times for the transition. In heat storage applications we recommend selecting conditions well away from the phase transition lines (at least outside the metastable zone) and to leave some seeds of the phase to be transferred in order to increase the transition speed.

1. Introduction

The mismatch between supply and demand is one of the main hurdles in the transition to renewable energy. This hurdle can be overcome by storing heat, especially in the domestic environment since 70% of energy is used for heating houses and hot water [1]. This requires a compact and safe method which can be provided by thermochemical heat storage. This method stores heat through the reversible chemical reaction between a thermochemical material (TCM) and a gas. The energy is stored in chemical bonds, which offers a large heat of reaction [2]. For use in residential areas water vapour is the preferred gas as it is safe and readily available, while the temperature required for the chemical reaction (particularly the dehydration) is limited to temperatures that can be reached with solar boilers for domestic use (maximum 150 °C) [3].

There are several salt hydrates that meet these criteria for a TCM. The heat is stored by dehydrating the salt and can be released by the reverse process of hydration. Examples of salts that have been studied in detail are K_2CO_3 [1,4,5], $CaCl_2$ [6,7], $MgCl_2$ [4,8–10], Na_2S [4] and $MgSO_4$ [8,11–13]. Most of these salt hydrates have a high energy density (e.g. K_2CO_3 1.28 GJ/m^3 [4] and hexa-to monohydrate $CaCl_2$ 2.16 GJ/m^3 [14]), but some have stability issues resulting in the release of toxic gas ($MgCl_2$ and Na_2S [4,15]), or rehydration issues due to limited water vapour transport ($MgSO_4$) [12].

Recently, strontium chloride has been identified as a possible candidate for domestic thermochemical heat storage [1,16]. This compound was reported to have a high theoretical energy density for the hexahydrate of 2.51 GJ/m^3 with respect to the anhydrate [17]. So far $SrCl_2$ has been used as an additive to improve the water vapour transfer in $MgSO_4$ by Li et al. [18] which gives full cyclic stability for this salt mixture. However, full cyclic stability of pure $SrCl_2$ has not been shown.[1] Other applications for $SrCl_2$ were in a composite material (pumice [20], activated carbon [21], silica gel [22] and cement [23]). Recent work by Clark et al. [24] studies the hydration kinetics (conversion speed) of the anhydrate to hexahydrate transition of $SrCl_2$, skipping intermediate hydration states, as well as its kinetics when used in a cement composite.

---

* Corresponding author.
** Corresponding author.
   E-mail addresses: h.p.huinink@tue.nl (H.P. Huinink), e.vlieg@science.ru.nl (E. Vlieg).
[1] After this paper was submitted, another publication became available which shows full cyclic stability for $SrCl_2$ [19].

Nomenclature

$\Delta_r G^0$	Molar Gibbs energy (J•mol^{-1})
R	Universal gas constant (8.314 J•mol^{-1}•K^{-1})
T	Temperature (K, °C)
K	Thermodynamic equilibrium constant (no unit)
a	Activity (no unit)
p:	Pressure (mbar)
p^0	The standard pressure (1000 mbar)
$\Delta_r H^0$	The standard molar reaction enthalpy (J•mol^{-1})
$\Delta_r S^0$	The standard molar reaction entropy (J•mol^{-1}•K^{-1})
$\Delta\mu$	The difference in chemical potential (J•mol^{-1})
t	Time (min)
HF	Heat flow (W•g^{-1})

Indices

SrCl$_2$	Anhydrous strontium chloride
H$_2$O	Water
(s)	Solid
(g)	Gas
eq	Equilibrium

SrCl$_2$ has multiple hydration states and it is chemically stable up to 250 °C [23]. However, a potential disadvantage is that the hexahydrate decomposes into a solution and its dihydrate at 61.3 °C, which can occur during dehydration. This process can be described as "melting" [25]. The salt has three reversible reaction steps from the hexahydrate through the di- and monohydrated states to the final SrCl$_2$ anhydrate.

The complete (p,T) phase diagram including all these phases of SrCl$_2$ has been calculated by Steiger based on thermodynamic data [17]. He concluded that the compound has great potential as a TCM, because it has a higher deliquescence humidity than MgCl$_2$ and CaCl$_2$ thus avoiding issues with solution formation [12,26]. Additionally, in contrast to several sulfates [27–30], SrCl$_2$ requires lower water vapour pressures to reach the final hydration state. Furthermore, the hydration of many sulfates is slow and results in incomplete hydration [13,31–34]. This does not apply to SrCl$_2$, as shown by Clark et al. [24].

In practical applications, however, kinetic effects such as nucleation and growth processes play a crucial role in the behaviour of any TCM. As a result, the temperature and water vapour pressure needed for a transition can deviate from the thermodynamic equilibrium values. The differences between equilibrium phase transition pressure and temperature and the actual transition values span what is called the metastable zone of the transition. Mapping out the metastable zone width (MZW) is therefore crucial for the application of salt hydrates in a heat battery, since it involves practical aspects such as the output temperature and the kinetics of the reaction [5,35].

Therefore, we need to understand the transitions of the salt to optimize the performance of a TCM in applications. The purpose of this work is to determine the properties of SrCl$_2$ as a TCM from a thermodynamic point of view by studying all its hydration and dehydration transitions. This also allows a comparison between these transitions for one and the same material. We experimentally determined the thermodynamic equilibria of each transition (phase equilibrium lines in a (p,T)-diagram, the phase transition enthalpies and entropies) and the kinetics of the separate transitions. The latter include determining the MZW, cyclability and induction times. The induction time is the time needed for a transition to start once the conditions are changed to invoke the transition.

2. Theory

The three hydration and dehydration reactions for SrCl$_2$ and its hydrates are given by:

These equations can be summarised into a general reaction equation by:

$$SrCl_2 \cdot nH_2O(s) \leftrightarrow SrCl_2 \cdot mH_2O(s) + (n-m)H_2O(g), \tag{1}$$
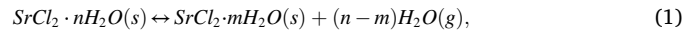
where n and m are the number of water molecules in the higher and lower hydrate, respectively.

This leads to the thermodynamic equilibrium constant K determined by

$$\Delta_r G^0 = -\mathrm{RT}\ln K = -RT\ln\frac{a(SrCl_2 \cdot mH_2O(s)) \cdot a^{n-m}(H_2O(g))}{a(SrCl_2 \cdot nH_2O(s))}$$
$$= -(n-m)\mathrm{RT}\ln\left(\frac{p}{p^0}\right), \tag{2}$$

where we set the activity a equal to one for the solids and assume perfect gas behaviour for the vapour. In this equation p is the water vapour pressure in mbar, p^0 the standard pressure (1000 mbar), $\Delta_r G^0$ the molar reaction Gibbs energy, R the gas constant and T the temperature in K. The reaction Gibbs energy for dehydration at temperature T can also be expressed as:

$$\Delta_r G^0 = \Delta_r H^0 - T\Delta_r S^0, \tag{3}$$

where $\Delta_r H^0$ is the standard molar reaction enthalpy (J•mol^{-1}) and $\Delta_r S^0$ the standard molar reaction entropy (J•mol^{-1}•K^{-1}). Substituting $\Delta_r G^0$ in eq. (2) gives the linear form of the Van 't Hoff equation which is valid for dehydration [36,37].

$$(n-m)\ln\left(\frac{p}{p^0}\right) = \frac{\Delta_r S^0}{R} - \left(\frac{\Delta_r H^0}{R}\right)\frac{1}{T}. \tag{4}$$

By dividing this equation by the number of water molecules involved in the reaction, $(n$-$m)$, it can be used to estimate the $\Delta_r H^0$ and $\Delta_r S^0$ of the different hydrate transitions per water molecule assuming that they are independent from the temperature.

The difference in chemical potential, $\Delta\mu$ (J•mol^{-1}), for a transition induced by changing the temperature T, starting from an equilibrium situation T_{eq}, is given by

$$\Delta\mu = RT\ln\frac{p_{eq}(T_{eq})}{p^0} - RT_{eq}\ln\frac{p_{eq}(T_{eq})}{p^0} = R(T - T_{eq})\ln\frac{p_{eq}(T_{eq})}{p^0}. \tag{5}$$

This equation shows that the initial difference in chemical potential per mole water driving the reaction (which is called the driving force in crystal growth theories) increases linearly with increasing or decreasing temperature for dehydration and hydration, respectively.

Similarly, the difference in chemical potential, $\Delta\mu$ (J•mol^{-1}), for a transition induced by changing the pressure P, starting from an equilibrium situation P_{eq}, is given by

$$\Delta\mu = RT_{eq}\ln\frac{p(T_{eq})}{p^0} - RT_{eq}\ln\frac{p_{eq}(T_{eq})}{p^0} = RT_{eq}\ln\frac{p(T_{eq})}{p_{eq}(T_{eq})}. \tag{6}$$

3. Materials and methods

3.1. Sample preparation

The SrCl$_2$ crystals were grown from powder (95% Alfa) dissolved in demi water prior to measurements to improve the purity. This resulted in needles of SrCl$_2$•6H$_2$O shown in Fig. 1, as confirmed with single crystal x-ray diffraction. The purity of the crystals was determined to be 99.45% by elemental analysis (ICP-OES). The main impurities are calcium (0.4%), magnesium (0.04%) and silicon (0.05%).

Experiments were also done with SrCl$_2$•6H$_2$O purchased from Fischer Scientific. This powder was sieved to 50–100 μm size fraction. The certificate of analysis of the SrCl$_2$•6H$_2$O (99+ %) from Fischer Scientific, showed it had a purity of 99.1%, but it was not specified what
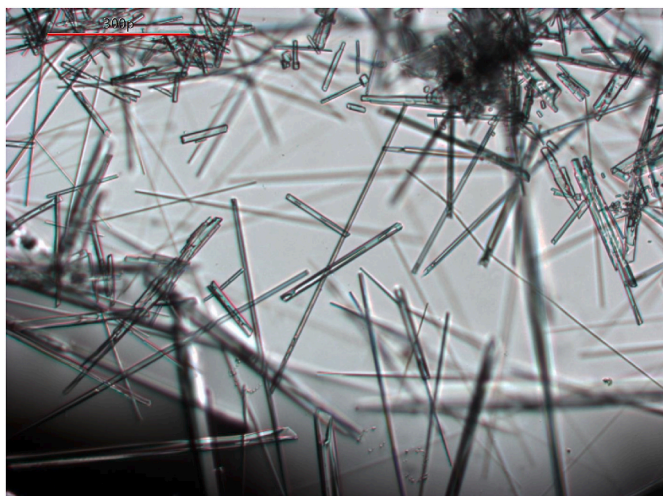
Fig. 1. Optical microscopy image of SrCl$_2$ hexahydrate needles. The line is 280 μm wide.

the impurities were. In our experiments, however, this small purity difference did not have any significant effect on the results, and this was found to be the case even in some experiments with the 95% purity material. We can thus exclude purity as a relevant parameter for our samples and will not discuss this any further.

The full hydration of single crystals was particularly relevant for the enthalpy determinations since we found the sample to dehydrate at ambient conditions. The powder is better suited for practical applications because it allows better water vapour and heat transport.

3.2. Pressure-temperature measurements

A *p,T*-meter set-up as described by Sögütoglu et al. [5] was used to measure the equilibrium phase lines of the SrCl$_2$–H$_2$O system. Approximately 1 g of SrCl$_2 \bullet n$H$_2$O was used, with "*n*" being the higher hydration state for the equilibrium line that was studied. The temperature was increased stepwise with sufficient time in between to reach an equilibrium water vapour pressure. The equilibrium vapour pressure line was constructed as a function of temperature based on these data points.

3.3. Enthalpy determination

The enthalpy per mol H$_2$O ($\Delta_r H^0/(n\text{-}m)$) was determined from the dehydration transitions with a differential scanning calorimeter (DSC) of type Mettler-Toledo DSC 3. Approximately 5 mg of SrCl$_2 \bullet 6$H$_2$O crystals were placed in a standard 40 μL aluminium pan with a closed lid and melted by heating it from 25 °C to 90 °C with a rate of 0.1 K/min, followed by cooling the sample to room temperature with a rate of −10 K/min. Subsequently the lid of the pan was pierced, and the sample was dehydrated in the DSC from −10 °C to 150 °C with a rate of 0.1 K/min. The transition peaks were integrated to obtain the enthalpy for each

transition.

3.4. Thermogravimetric analysis

Set-up and humidity conditioning: The amount of water released in time was determined with a thermogravimetric analyser (TGA) of type Mettler-Toledo TGA/DSC 3+ which was equipped with a humidity controller (Fig. 2). The humidity is controlled by heating a water bath to a set temperature, thus creating water vapour with 100% relative humidity at the temperature of the water bath and well-defined partial pressure. This gas is then mixed with a dry N$_2$-flow at a set ratio. The gas flow was limited to 250 mL/min to minimize the temperature difference between the sample and the reference pans, since the gas is approximately at room temperature and flows over the sample pan while adopting the temperature of the oven. The partial water vapour pressure of the gas mixture was calibrated with the deliquescence points of LiCl, CaBr$_2$, MgCl$_2$, CoBr$_2$ and NaBr. The estimated error of the calibration is ±1.1 mbar. Approximately 10 mg of SrCl$_2$ powder was placed in a standard 100 μL aluminium pan without a lid. The temperatures and heating rates were different for each type of experiment.

Metastable zone: Metastable zone width (MZW) values were measured using TGA, by cooling and heating the salt at a fixed water vapour pressure and detecting the onset temperature of the sample at a cooling/heating rate of 0.1 K/min. The samples used were either single crystals (sc) or 99% pure SrCl$_2 \bullet 6$H$_2$O powder.

Induction times: The induction times were measured using TGA by first pre-treating the SrCl$_2$ by keeping it at *p,T*-conditions required for the desired hydration state for 1 h (unless otherwise specified). Once the SrCl$_2$ was in the desired hydration state, the temperature was rapidly (20 K/min) changed to one where a transition is expected. The temperature was then kept constant to allow the transition to occur (for example: 12 mbar water vapour pressure with 1 h dehydration to anhydrate at 130 °C followed by 8 h at 70 °C to see the transition to monohydrate). This was repeated for several temperatures at one fixed water vapour pressure and for several water vapour pressures for one set temperature. The induction time was measured from the point where the desired temperature and pressure were reached until the onset of the transition.

Cyclic measurements: The cyclability was tested by dehydrating a powder sample for 4 h at 130 °C followed by 6 h of hydration at 25 °C, both at a fixed water vapour pressure of 22 mbar. This entire process was done ten times consecutively with a cooling/heating rate of 10 K/min.

4. Results & discussion

4.1. Phase diagram and metastable zones

In Fig. 3, the phase behaviour for the SrCl$_2$–H$_2$O system is presented. The experimental equilibrium data as determined using the (*p,T*)-meter are represented by the filled circles. The theoretical equilibrium lines between the various phases (dashed lines in the diagram) are from the work by Steiger [17]. The dotted lines are from the work of Clark et al. [24] which is based on the enthalpy data from Gmelin [38] but further
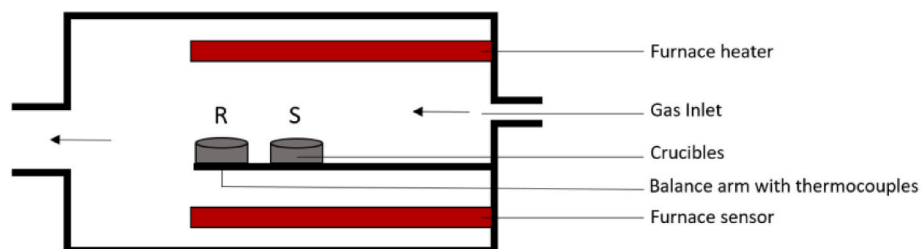
Fig. 2. Schematic representation of TGA/DSC. There are two crucibles, the empty reference crucible (R) and the crucible with sample (S). The oven is cooled and heated with typical rate of 0.1 K/min (for MSZ) while humidity inside the oven is controlled with a gas flow with set partial water vapour pressure.
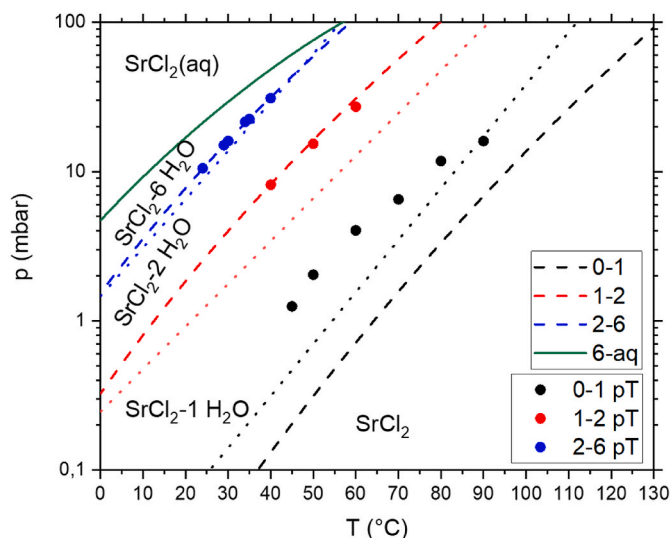
Fig. 3. Experimental phase diagram of SrCl$_2$, plotted as partial water vapour pressure vs. temperature. The experimental equilibrium pressures determined with the p,T-meter are indicated with the full circles and the lines represent the equilibria from literature; dashed Steiger [17] and dotted Clark et al. [24].

Fig. 4. Experimental phase diagram, partial water vapour pressure vs. temperature, of SrCl$_2$. The dashed lines represent the deliquescence equilibrium and hydration equilibria from literature [17]. The filled circles represent the experimental equilibrium pressures determined using the (p,T)-meter. The triangles directed to the left represent the onset temperatures for hydration and the triangles directed to the right for dehydration. The triangles are open (99% powder sample) or half-filled (single crystal sample). The metastable zone is indicated with grey for 0–1 transition, red for 1–2 transition and blue for the 2–6 transition. (For interpretation of the references to colour in this figure legend, the reader is referred to the Web version of this article.)

used unspecified offset data for the lines. The differences clearly demonstrate the sensitivity of the theoretical lines for the parameter values used. Due to the logaritmic nature of equation (4), deviations of the order of 2.5 kJ/mol, which are minor variations for $\Delta_r H^0/(n\text{-}m)$, lead to a significant difference.

The experimental values of the 2–6 transition confirm the theoretical predictions well. Further, the experimental values of the 1–2 transitions overlap well with the data from Steiger, but not with Clark et al. As only the source for the enthalpy they used was specified in their paper and no further data for the offset of the lines, there is no way to explain the large deviation.

For the 0–1 transition there is a clear difference between experimental and theoretical data. While there were some experimental limitations (at the highest temperatures equilibrium might not have been reached), the location of the experimental p,T line is expected to be reliable. Note that Steiger's approach extrapolates the equilibrium line from the behaviour of concentrated solutions, which will be prone to error at very low water activities. Additionally, this particular line was based on experimental data of limited quality [39]. Once more, the data for the offset of the line used by Clark et al. was not specified in their paper.

Metastable zone width (MZW) values were measured using TGA. The samples used were either single crystals (indicated in Fig. 4 as sc) or SrCl$_2$•6H$_2$O powder (in Fig. 4 indicated as pw). Based on Fig. 4, a clear difference was found between the MZWs for the various transitions. The MZW for the 0–1 transition is about 55 K, while the MZW for the 1–2 transition is about 20 K and the MZW for the 2–6 transition is about 5 K (at 20 mbar).

The 1–2 metastable zone is symmetrical with respect to its equilibrium line. The 2–6 metastable zone is asymmetrical with the dehydration happening at the equilibrium, but a small MZW for the hydration. The experimental p,T data for the 0–1 transition are located more in the centre of the metastable zone in contrast to the theoretical equilibrium line. However, given the uncertainty in the position and slope of the theoretical line [39], it can be concluded that the 0–1 transition is reasonably symmetrical around the equilibrium data points.

Overall, the MZW decreases for higher hydration content transitions. This might be related to the wetting layer at the surface of the crystals, which is expected to increase in thickness with higher supersaturations of water vapour pressures [5,35]. However, this has not been experimentally verified or quantified for SrCl$_2$. An alternative explanation for

the width of the 0–1 metastable zone is the huge change in crystal structure which goes from cubic Fm $\overline{3}$ m to orthorhombic Pnma. Either of these explanations will need to be tested.

4.2. Transition enthalpy and entropy

4.2.1. DSC experiment results

Single crystals were taken directly from solution to ensure we had fully hydrated hexahydrate sample for enthalpy determination in the DSC. The pan was sealed directly after weighing the sample which was required because the hexahydrate dehydrates at ambient conditions (with a relative humidity that can be below 30% in our lab). The lid was pierced right before the DSC experiment. We learned that limited water vapour transport occurs inside a pan with a pierced lid when the heating rate is 0.5 K/min, especially with a large sample (11.4 mg). This leads to overlapping dehydration and incongruent melting as shown in Fig. 5 with the black line.

When the sample pan remains fully sealed during heating in the DSC the water will remain liquid, thus partially dissolving the SrCl$_2$ in its own crystal water at 61.3 °C, a process also described as melting of the SrCl$_2$ hexahydrate [25] and illustrated by the red line in Fig. 5. Subsequent piercing of the lid and then heating the sample with a slower rate of 0.1 K/min gives clear distinct dehydration peaks (green line).

Virtually the same result can be obtained by using a pan with pierced lid and dehydrating a smaller sample of 5 mg with a heating rate of 0.1 K/min without "melting" prior to the dehydration process (not shown in Fig. 5 since it would overlap with green line). This shows that melting and recrystallisation does not have any adverse effect on the dehydration process. The dehydration experiments were done in triplicate to determine the transition enthalpies. The average of these three measurements is given in Table 1. The total energy density for a 0–6 transition was calculated to be 2.4 ± 0.1 GJ/m^3 based on the density of the SrCl$_2$•6H$_2$O, which is in good agreement with the value of 2.51 GJ/m^3 reported by Steiger [17].

4.2.2. Enthalpy values comparison

Next we compare the enthalpy values from the experiments (both
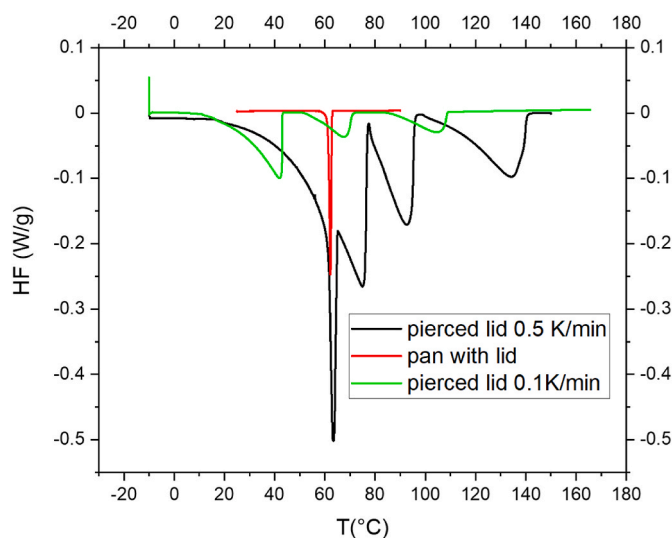
Fig. 5. DSC results of heating of $SrCl_2$ hexahydrate with a pierced lid with 0.5 K/min heating rate (black), closed lid showing melting only (red) and a subsequently pierced lid with a 0.1 K/min heating rate (green). (For interpretation of the references to colour in this figure legend, the reader is referred to the Web version of this article.)

Table 1
Standard molar enthalpy of dehydration per mole water for the various transitions for the $SrCl_2$ hydrates.

$\Delta_r H^0/(n\text{-}m)$ per transition	6-2 [kJ/mol H_2O]	2-1 [kJ/mol H_2O]	1-0 [kJ/mol H_2O]
DSC results	50 ± 6.2	60 ± 2.7	63 ± 3.5
p,T results	53 ± 1.5	58 ± 2.3	54 ± 9.0
DSC Gmelin [38]	54	59	68
Steiger fit [17]	54	58	76
DFT calculations [41]	56	55	60

DSC and *p,T* experiments) with earlier DSC results [40], Steiger's work [17], DFT calculations [41] and thermodynamic calculations [37]. The equilibrium lines from Steiger as well as the data determined from the *p,T* measurements were fitted to equation (4) to determine the enthalpy for each transition. All data are shown in Table 1.

The experimental fit results for the 6-2 and 2-1 transitions are close to the value of the fit to Steiger's data, which was expected since the data overlapped in Fig. 3. Also, both the 6-2 and 2-1 transitions, agree quite well (±5 kJ/mol) with the other literature data (previous DSC and DFT calculations).

However, for the 1-0 transition this is not the case. Our *p,T*-data has a wide error range for this transition due to the aforementioned experimental difficulties. The error in the enthalpy was estimated by first fitting all data points and comparing this with the values when using 4 out of 6 data points in different combinations. The DFT calculations and our DSC results agree reasonably well. However, Steiger's values are a lot higher than the experimental DSC and *p,T* values. This is most likely due to the aforementioned extrapolation from saturated solution to very low water activities and the limited quality of the experimental data used [39]. There is a moderate increase in enthalpy per mole of water when going to lower hydration states. However, the 6-2 transition has by far the largest enthalpy difference since it has 4 mol of water in the transition.

4.2.3. Entropy values comparison

The entropy values for the different transitions are given in Table 2. Once more we fitted the equilibrium lines from Steiger as well as the data determined from the *p,T* measurements to equation (4) to

Table 2
Entropies of the various transitions for the $SrCl_2$ hydrates.

ΔS per transition	6-2 [J•mol^{-1}•K^{-1}]	2-1 [J•mol^{-1}•K^{-1}]	1-0 [J•mol^{-1}•K^{-1}]
p,T results	139 ± 5	126 ± 7	116 ± 27
Steiger fit [17]	142	146	169
Glasser [37]	146	91	184

determine the standard molar entropy for dehydration for each transition. For the 6-2 transition the *p,T* results and the literature values are in good agreement. In the case of the 2-1 transition, there were only three datapoints so the fit for the entropy has a large uncertainty. The entropy obtained from Steiger is more in agreement with our value. The entropy value from Glasser for this transition is unexpectedly low. It is unclear why this is the case; Glasser used the HSC chemistry database in his paper, but it lacks information on how these values were obtained.

Finally, for the 1-0 transition there is an even larger discrepancy between our value and the literature values, even when taking into account the large uncertainty in this case due to the scattering in our experimental *p,T* values. However we are convinced our experimental *p, T* data gives the most reliable value for the entropy since it gives a reliable indication for the position of the *p,T* line. Steiger's values for this transition are based on unreliable experimental values [39] and as mentioned before it is unclear what Glasser's entropy value is based on.

4.3. Induction times

4.3.1. Fixed water vapour pressure and varied temperatures

A systematic study of the induction times for the hydration and dehydration transitions has been performed. For an overview of all experimental conditions (*p,T*) we refer to Fig. 6. The conditions are indicated in the phase diagram and labelled with the number of minutes it took for the transition to start.

A. Hydration: The hydration is shown in the left panel of Fig. 6. For the hydration of the anhydrate (black symbols) we see the induction times decrease with decreasing temperatures with one outlier at 70 °C and 22 mbar which has an induction time of 9 min. Interestingly, at 50 °C and 22 mbar the dihydrate could be formed according to the phase diagram, but instead the anhydrate did not continue hydrating (within 8 h) after the monohydrate was formed. In the case of the hydration of the monohydrate to the dihydrate (red symbols) we see no clear correlation between induction time and temperature. The hydration from dihydrate to hexahydrate had a short induction time, but we could not obtain data at lower temperatures due to condensation issues.

B. Dehydration: The dehydration is shown in Fig. 6 on the right. The dehydration of the hexahydrate to the dihydrate (blue triangles) started fast for all tested conditions. The dihydrate took a long time to start dehydrating if at all. However, at low *p* the induction time increased with the temperature. Finally, the monohydrate also took a long time to start dehydrating except for the measurement at 110 °C and 22 mbar.

We expected the hydration to go faster for lower temperatures and for the dehydration we were expecting it to go faster for higher temperatures. However, this was not observed. To find out what caused this unexpected result we did a series of reproducibility experiments in which we aimed to have improved control over the conditions.

C. Reproducibility hydration anhydrate to monohydrate: We did these reproducibility experiments for the hydration of the anhydrate to the monohydrate at $p = 22$ mbar and $T_r = 70$ °C (i.e., the condition of the previously mentioned outlier with an original induction time of 9 min), because the anhydrate is the form that is the easiest to prepare. The results are shown in Fig. 7 for two different preparations
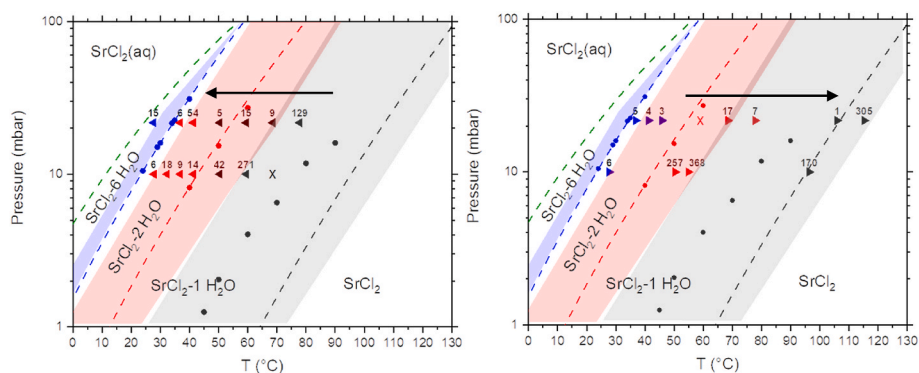
Fig. 6. The kinetic experiments on induction times at their corresponding p and T are indicated in the phase diagrams of SrCl$_2$–H$_2$O. On the left: The hydration experiments. On the right: the dehydration experiments. X means the experiment did not result in a transition within 8 h, otherwise the number above the point indicates the induction time in minutes. Blue is used to indicate the transition between the di- and hexahydrate, red for the transition between mono- and dihydrate and black for the transition between the anhydrate and monohydrate. (For interpretation of the references to colour in this figure legend, the reader is referred to the Web version of this article.)
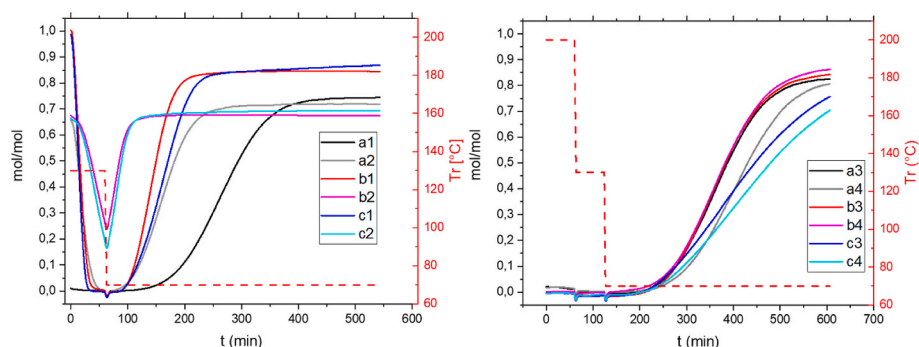
Fig. 7. Reproducibility experiments. All experiments were done at a constant water vapour pressure of 22 mbar. The temperature profiles are indicated with the red dashed line. Left: with preheating for 1 h at 130 °C and right: with added preheating for 1 h at 200 °C. (For interpretation of the references to colour in this figure legend, the reader is referred to the Web version of this article.)

conditions of the anhydrate. Three powder samples (a, b and c) were prepared and each went consecutively through the same four temperature programmes (labelled 'a1'- 'a4' in the legend to Fig. 7). The experiments at $T_r = 70$ °C showed that the induction times are highly dependent on the pre-treatment of the sample. It is clear that dehydrating the sample at 130 °C for 1 h is insufficient to ensure complete dehydration (Fig. 7 left panel), because the induction time was a lot shorter in the second round (a2). This is probably due to some remaining seeds of the desired end state (in this case the monohydrate) from a previous experiment, even though the sample weight indicated that the desired initial state (anhydrate) was achieved. The dehydration was incomplete for experiments b2 and c2 at these conditions. Another experimental complication is the formation of an inactive or caked layer at the top of the sample, blocking full hydration of the sample which makes it difficult to get to the desired starting hydration state (other than the anhydrate). This can be seen in Fig. 7 (left panel) where hydration appears to stop at 0.7 mol H$_2$O for 4 experiments.

D. Reproducibility hydration anhydrate to monohydrate with preheating at 200 °C: Repeating these experiments with a preheating temperature of 200 °C (Fig. 7 right panel) is found to be enough to remove any seeds of the monohydrate and resulted in an induction time of 123 ± 16 min with a smaller spread between the different experiments (original spread was 120 min). Additionally, we tested the reproducibility for $p = 22$ mbar and $T_r = 65$ °C using the same 200 °C preheating. This led to faster induction times of 31 ± 6 min. This corresponds with our expectations since lowering the temperature increases the $\Delta\mu$ for hydration.

In summary, the wide spread between the induction times (9–120 min) in Figs. 6 and 7 (left panel) is due to the preparation conditions which turned out to be insufficient to remove all monohydrate seeds,

even though TGA data suggested full dehydration. When the preparation ensures all seeds of the monohydrate are removed, the spread in induction times is moderate (Fig. 7 right panel and the experiments at 65 °C) and is due to the stochastic nature of nucleation.

Such stochasticity is typically found in crystal nucleation experiments in solution [42]. In solution growth the number of nucleation events is typically small and thus the spread in induction times large, especially at low supersaturations. In our powder there are a lot of crystals with each grain having their own defects. Due to this wide range of conditions in a powder sample the odds of one grain transitioning are increased. The initial nucleation does not lead to instant transition of the other crystals in the sample, as shown by the variation in slopes in Fig. 7 (right panel). This is similar to other solid state transitions in single crystals, where a transition starts at one or more defects and it takes a while before the entire crystal has transitioned [43].

4.3.2. Fixed temperature and varied water vapour pressure

An alternative way of changing the $\Delta\mu$ for hydration is by adjusting the water vapour pressure at constant temperature (see equation (6)). In this case we expect a lower water vapour pressure to lead to a longer induction time. This was tested for 5 different water vapour pressures at

Table 3
Induction time for the nucleation of the anhydrate to the monohydrate at different water vapour pressures.

Water vapour pressure [mbar]	Temperature 70 °C: Induction times [min]	Temperature 65 °C: Induction times [min]
22	131	26
19	319	77
17	>480	183
15	>480	>480
12	>480	>480

two different temperatures as shown in Table 3. We ensured the initial state was the anhydrate by preheating the sample to 200 °C just like in the reproducibility experiments. The results agree with our expectation, showing that even a slight decrease in water vapour pressure results in a significantly longer induction time. Times exceeding the duration of the experiment are indicated with >480 in the table. These experiments were done once, however, we assume these results to be indicative of the nucleation time (within a certain spread) since the preheating at 200 °C ensures complete removal of monohydrate seed crystals.

4.4. Cyclability

Li et al. [18] observed decreased water uptake in subsequent cycles when pure $SrCl_2$ is cycled. However, they used short hydration and dehydration times of 20 min. In contrast, we let the sample dehydrate for 4 h and hydrate for 6 h, which resulted in full reversibility without chemical degradation for at least 10 cycles (Fig. 8). The different cycles overlap well, proving the reproducibility of the process.

In all cycles, during the heating (10 K/min), the dehydration from hexahydrate to monohydrate happens without visible pause at the dihydrate intermediate. The pause at the monohydrate coincides with the end of the heating slope. After this point the dehydration to the anhydrate continues at a slower pace, because the driving force for the transition to the anhydrate is lower under these conditions than the driving forces for the 6-2 and 2-1 transitions were.

For the hydration a slight difference is observed between the first hydration from dihydrate to hexahydrate (black line) as compared to the 2nd to 10th hydrations (other lines). The hydration goes slightly faster the first time. The hydration to the monohydrate is completed during the cooling (10 K/min), the hydration then continues with the same speed at 25 °C until the dihydrate is reached. The speed of transition decreases between the dihydrate to the hexahydrate, resulting in a kink in the graph at a loading of 2 mol water per $SrCl_2$. The conversion rates of these transitions in mol/min are approximated by a linear fit and given in Table 4. This approximation does confirm Clark et al.'s [24] observation that the hydration from the dihydrate to the hexahydrate is the slowest step. This follows from eq (6) which shows that $\Delta\mu$ is proportional to $ln\frac{p(T_{eq})}{p_{eq}(T_{eq})}$. The equilibrium vapour pressure for the 6-2 transition is much higher than for the 2-1 and 1-0 transitions. In contrast to Clark et al. we could observe the hydration from the anhydrate (through the
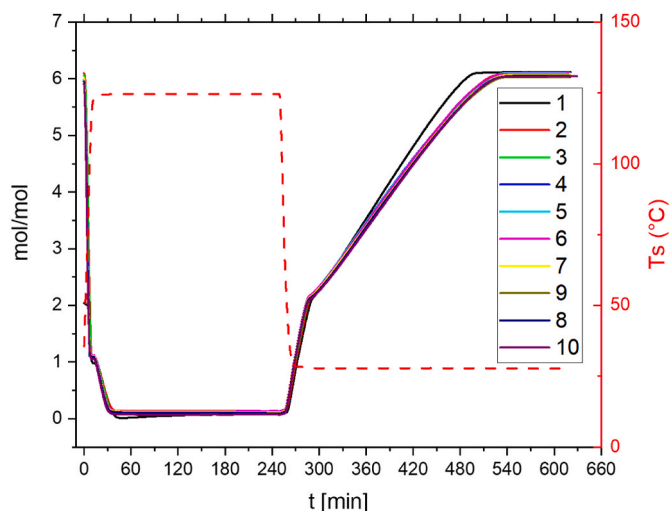
Fig. 8. Cyclability of $SrCl_2$ from anhydrate to hexahydrate at p = 22 mbar. The loading in mol H_2O per mol $SrCl_2$ is shown on the left y-axis and the solid lines, one per cycle. The sample temperature (Ts) is shown on the right y-axis and the red dashed line. (For interpretation of the references to colour in this figure legend, the reader is referred to the Web version of this article.)

Table 4
Conversion rates of the different transitions at 22 mbar.

Transition	Conversion rate (mol/min) $\pm$ 95% confidence interval
6–1	0.50 $\pm$ 0.03
1–0	0.040 $\pm$ 0.003
0–2	0.063 $\pm$ 0.002
2–6	0.017 $\pm$ 0.0007

monohydrate) to the dihydrate. This transition is about three times faster than the di-to hexahydrate transition, in our experimental conditions. This can be partly explained by the fact that the driving force for the 2–6 transition at this temperature and water vapour pressure is smaller than for the other two (see eq. (5)).

4.5. Comparison $SrCl_2$ with other salt hydrates for heat storage

Multiple reviews [1,14] have summarised and assessed the use of different pure salts for heat storage, most recently Li et al. [44]. That review refers to several well-studied salt hydrates for application as TCMs like NaS_2, $MgCl_2$, $MgSO_4$, $SrBr_2$ and K_2CO_3. However, as mentioned in the introduction, NaS_2 and $MgCl_2$ are chemically instable [4] while $MgSO_4$ shows poor rehydration kinetics [10]. As demonstrated in this paper, $SrCl_2$ does show chemical and cyclic stability. Meanwhile its energy density (2.5 GJ/m^3) is confirmed to be higher than that of $SrBr_2$ and K_2CO_3 (1.93 [14] and 1.3 GJ/m^3 [4], respectively). Thus, compared to these well-studied cases, we find that $SrCl_2$ has favourable characteristics for all parameters that are important for heat storage.

5. Conclusion

We have demonstrated that $SrCl_2$ can completely and reversibly cycle from anhydrate to hexahydrate for at least 10 cycles without chemical degradation. In these cycles the hydration from dihydrate to hexahydrate is the slowest step, yet hydration within 6 h is possible. Additionally, the experimental total energy density of 2.4 $\pm$ 0.1 GJ/m^3 corresponds well to the theoretical value from the literature (2.51 GJ/m^3). This high energy density is an advantage over other salts, like K_2CO_3 which is already being used in applications.

Furthermore, we have established that the $SrCl_2$–H_2O system has MZWs for the 0–1, 1–2 and 2–6 transitions of respectively 55, 20 and 5 K for cooling/heating rates of 0.1 K/min. These MZWs decrease with higher water content transitions. The 2–6 transition only has a MZW for the hydration, the dehydration happens at the equilibrium. In contrast, the 1–2 transition has a symmetrical metastable zone. The measured 0–1 equilibrium (p,T) data points lie reasonably well in the middle of the metastable zone of this transition.

The enthalpy per transition was experimentally determined in the DSC and with p,T experiments and varies from 50 to 63 kJ/mol H_2O. The experimental values correspond well with literature values, except for the 0–1 transition for which the uncertainty is somewhat larger. The enthalpy per mole increases with decreasing hydration state, but the highest enthalpy is in the 6-2 transition since it has 4 mol of water. Our experimental entropy values are surrounded by some uncertainty but do appear to be in range with the previously reported mean value of 146 J•mol^{-1}•K^{-1}.

Finally, we have established that the induction times are highly dependent on the preparation conditions of the sample. When the sample is carefully prepared it is possible to eliminate precursor seeds and then the induction times decrease with increasing $\Delta\mu$. Remaining seeds will decrease the induction times, which is favourable for practical applications. Additionally, a water vapour pressure and temperature outside of the MSZ can be chosen to facilitate rapid transitions. Both the cyclic stability and density confirm the suitability of $SrCl_2$ for heat storage.

A challenge for using this compound in practical applications is the

high water vapour pressure required to transition to the hexahydrate and thereby obtaining the full potential for the energy density. Another challenge is ensuring water vapour transport does not get limited during dehydration which can lead to incongruent melting. This did not lead to issues on our mg scale with open pans but should be taking into account when designing a device.

Nevertheless, both the cyclic stability and heat density confirm the suitability of $SrCl_2$ for heat storage.

CRediT authorship contribution statement

Melian A.R. Blijlevens: Writing – original draft, Visualization, Validation, Resources, Project administration, Methodology, Investigation, Formal analysis, Data curation, Conceptualization. **Natalia Mazur:** Investigation. **Wessel Kooijman:** Validation. **Hartmut R. Fischer:** Conceptualization, Writing – review & editing. **Henk P. Huinink:** Writing – review & editing, Funding acquisition, Conceptualization. **Hugo Meekes:** Conceptualization, Funding acquisition, Supervision, Writing – review & editing. **Elias Vlieg:** Writing – review & editing, Supervision, Funding acquisition, Conceptualization.

Declaration of competing interest

The authors declare that they have no known competing financial interests or personal relationships that could have appeared to influence the work reported in this paper.

Acknowledgements

Appendix A. Supplementary data

Supplementary data to this article can be found online at https://doi.org/10.1016/j.solmat.2022.111770.

References

[1] P.A.J. Donkers, et al., A review of salt hydrates for seasonal heat storage in domestic applications, Appl. Energy 199 (2017) 45–68.

[2] M. Goldstein, Some Physical Chemical Aspects of Heat Storage by/Martin Goldstein, 1961, p. 7.

[3] L. Scapino, et al., Energy density and storage capacity cost comparison of conceptual solid and liquid sorption seasonal heat storage systems for low-temperature space heating, Renew. Sustain. Energy Rev. 76 (2017) 1314–1331.

[4] L.C. Sogutoglu, et al., In-depth investigation of thermochemical performance in a heat battery: cyclic analysis of K2CO3, MgCl2 and Na2S, Appl. Energy 215 (2018) 159–173.

[5] L.C. Sogutoglu, et al., Understanding the hydration process of salts: the impact of a nucleation barrier, Cryst. Growth Des. 19 (4) (2019) 2279–2288.

[6] P.A.J. Donkers, O.C.G. Adan, D.M.J. Smeulders, *Hydration/dehydration Processes in Stabilized CaCl2.* Poromechanics Vi, Proceedings of the Sixth Biot Conference on Poromechanics, 2017, pp. 656–663.

[7] M. Molenda, et al., Reversible hydration behavior of CaCl2 at high H2O partial pressures for thermochemical energy storage, Thermochim. Acta 560 (2013) 76–81.

[8] V.M. van Essen, et al., Characterization of salt hydrates for compact seasonal thermochemical storage. Es2009, in: Proceedings of the Asme 3rd International Conference on Energy Sustainability vol. 2, 2009, pp. 825–830.

[9] K. Posern, C. Kaps, Calorimetric studies of thermochemical heat storage materials based on mixtures of MgSO4 and MgCl2, Thermochim. Acta 502 (1–2) (2010) 73–76.

[10] P.A.J. Donkers, et al., Water transport in MgSO4 center dot 7H(2)O during dehydration in view of thermal storage, J. Phys. Chem. C 119 (52) (2015) 28711–28720.

[11] G. Whiting, et al., Heats of water sorption studies on zeolite-MgSO4 composites as potential thermochemical heat storage materials, Sol. Energy Mater. Sol. Cell. 112 (2013) 112–119.

[12] C.J. Ferchaud, et al., Study of the reversible water vapour sorption process of MgSO4 center dot 7H(2)O and MgCl2 center dot 6H(2)O under the conditions of seasonal solar heat storage, 2012, in: 6th European Thermal Sciences Conference, Eurotherm, 2012, p. 395.

[13] V.M. van Essen, et al., Characterization of MgSO(4) hydrate for thermochemical seasonal heat storage, J. Solar Energy Eng-Trans. Asme 131 (4) (2009).

[14] K.E. N'Tsoukpoe, et al., A systematic multi-step screening of numerous salt hydrates for low temperature thermochemical energy storage, Appl. Energy 124 (2014) 1–16.

[15] M. Roelands, et al., Preparation & characterization of sodium sulfide hydrates for application in thermochemical storage systems, 2014, in: International Conference on Solar Heating and Cooling for Buildings and Industry, Shc vol. 70, 2015, pp. 257–266.

[16] Z. Iyimen-Schwarz, M.D. Lechner, Energiespeicherung durch chemische reaktionen. I. DSC-messungen zur quantitativen verfolgung der enthalpieänderungen von speicherstoffen für die hin- und rückreaktion, Thermochim. Acta 68 (2) (1983) 349–361.

[17] M. Steiger, Thermodynamic properties of SrCl2(aq) from 252 K to 524 K and phase equilibria in the SrCl2-H2O system: implications for thermochemical heat storage, J. Chem. Thermodyn. 120 (2018) 106–115.

[18] W. Li, M. Zeng, Q.W. Wang, Development and performance investigation of MgSO4/SrCl2 composite salt hydrate for mid-low temperature thermochemical heat storage, Sol. Energy Mater. Sol. Cell. (2020) 210.

[19] R.-J. Clark, et al., Experimental screening of salt hydrates for thermochemical energy storage for building heating application, J. Energy Storage 51 (2022).

[20] A. Mehrabadi, M. Farid, New salt hydrate composite for low-grade thermal energy storage, Energy 164 (2018) 194–203.

[21] K. Posern, A. Osburg, Determination of the heat storage performance of thermochemical heat storage materials based on SrCl2 and MgSO4, J. Therm. Anal. Calorim. 131 (3) (2018) 2769–2773.

[22] J.J. Zhu, et al., Low-priced stable SrCl2@SG composite sorbents for low-grade solar heat storage application in open sorption systems, Sol. Energy Mater. Sol. Cell. (2021) 229.

[23] R.-J. Clark, M. Farid, Experimental investigation into the performance of novel SrCl2-based composite material for thermochemical energy storage, J. Energy Storage 36 (2021).

[24] R.-J. Clark, M. Farid, Hydration reaction kinetics of SrCl2 and SrCl2-cement composite material for thermochemical energy storage, Sol. Energy Mater. Sol. Cell. 231 (2021), 111311.

[25] C.W.F.T. Pistorius, Polymorphism and incongruent melting of SrCl2 · 6H2O to 50 kilobars, Z. Phys. Chem. 31 (3_4) (1962) 155–160.

[26] V.M. van Essen, J. Cot Gores, L.P.J. Bleijendaal, H.A. Zondag, R. Schuitema, M. Bakker, W.G.J. van Helden, in: Proceedings 3rd International Conference of Energy Sustainability, ASME, San Francisco, 2009.

[27] F. Hoffler, I. Muller, M. Steiger, Thermodynamic properties of ZnSO4(aq) and phase equilibria in the ZnSO4-H2O system from 268 K to 373 K, J. Chem. Thermodyn. 116 (2018) 279–288.

[28] F. Hoffler, M. Steiger, Thermodynamic properties of CuSO4(aq) from 268 K to 377 K and phase equilibria in the CuSO4-H2O system, Monatshefte Fur Chemie 149 (2) (2018) 369–379.

[29] K. Posern, et al., Thermochemical investigation of the water uptake behavior of MgSO4 hydrates in host materials with different pore size, Thermochim. Acta 611 (2015) 1–9.

[30] M. Steiger, et al., Decomposition reactions of magnesium sulfate hydrates and phase equilibria in the MgSO4-H2O and Na+-Mg2+-Cl–SO42–H2O systems with implications for Mars, Geochem. Cosmochim. Acta 75 (12) (2011) 3600–3626.

[31] P.A.J. Donkers, L. Pel, O.C.G. Adan, Experimental studies for the cyclability of salt hydrates for thermochemical heat storage, J. Energy Storage 5 (2016) 25–32.

[32] K. Linnow, et al., Experimental studies of the mechanism and kinetics of hydration reactions, in: Proceedings of the 2nd International Conference on Solar Heating and Cooling for Buildings and Industry (Shc 2013) 48, 2014, pp. 394–404.

[33] K. Posern, C. Kaps, Humidity controlled calorimetric investigation of the hydration of MgSO4 hydrates, J. Therm. Anal. Calorim. 92 (3) (2008) 905–909.

[34] M. Steiger, et al., Hydration of MgSO4 center dot H2O and generation of stress in porous materials, Cryst. Growth Des. 8 (1) (2008) 336–343.

[35] L.C. Sogutoglu, et al., Hydration of salts as a two-step process: water adsorption and hydrate formation, Thermochim. Acta (2021) 695.

[36] J. Stengler, J. Weiss, M. Linder, Analysis of a lab-scale heat transformation demonstrator based on a gas-solid reaction, Energies 12 (12) (2019).

[37] L. Glasser, Thermodynamics of inorganic hydration and of humidity control, with an extensive database of salt hydrate pairs, J. Chem. Eng. Data 59 (2) (2014) 526–530.

[38] Handbuch der Gmelin, Anorganischen Chemie, Verlag Chemie, Weinheim, 1966.

[39] M. Steiger, in: H. Meekes, M.A.R. Blijlevens (Eds.), Personal Communication; Online Presentation on Calculation of Phase Equilibria of Hydrated Salts, TCM meeting TUE, 2021.

[40] Z. Iyimen-Schwarz, M.D. Lechner, Energiespeicherung durch chemische reaktionen. I. DSC-messungen zur quantitativen verfolgung der enthalpieänderungen von speicherstoffen für die hin- und rückreaktion, Thermochim. Acta 68 (1983) 349–361.

[41] S. Kiyabu, et al., Computational screening of hydration reactions for thermal energy storage: new materials and design rules, Chem. Mater. 30 (6) (2018) 2006–2017.

[42] S.F. Jiang, J.H. ter Horst, Crystal nucleation rates from probability distributions of induction times, Cryst. Growth Des. 11 (1) (2011) 256–261.

[43] M.M.H. Smets, et al., Polymorphism of the quasiracemate D-2-aminobutyric acid: L-norvaline, CrystEngComm 19 (37) (2017) 5604–5610.

[44] W. Li, et al., Salt Hydrate-Based Gas-Solid Thermochemical Energy Storage: Current Progress, Challenges, and Perspectives, vol. 154, Renewable & Sustainable Energy Reviews, 2022.